

# Dilepton distributions at backward rapidities

M.A. Betemps<sup>1,2,\*</sup>, M.B. Gay Ducati<sup>1,†</sup> and E.G. de Oliveira<sup>1‡</sup>

<sup>1</sup> *High Energy Physics Phenomenology Group (GFPAE),  
Instituto de Física, Universidade Federal do Rio Grande do Sul,  
Caixa Postal 15051, CEP 91501-970, Porto Alegre, RS, Brazil*

<sup>2</sup> *Conjunto Agrotécnico Visconde da Graça, CAVG,  
Universidade Federal de Pelotas, Caixa Postal 460,  
CEP 96060-290, Pelotas, RS, Brazil*

(Dated: February 24, 2018)

## Abstract

The dilepton production at backward rapidities in  $pAu$  and  $pp$  collisions at RHIC and LHC energies is investigated in the dipole approach. The results are shown through the nuclear modification ratio  $R_{pA}$  considering transverse momentum and rapidity spectra. The dilepton modification ratio presents interesting behavior at the backward rapidities when compared with the already known forward ones, since it is related with the large  $x$  kinematical region that is being probed. The rapidity dependence of the nuclear modification ratio in the dilepton production is strongly dependent on the Bjorken  $x$  behavior of the nuclear structure function ratio  $R_{F_2} = F_2^A/F_2^p$ . The  $R_{pA}$  transverse momentum dependence at backward rapidities is modified due to the large  $x$  nuclear effects: at RHIC energies, for instance, the ratio  $R_{pA}$  is reduced as  $p_T$  increases, presenting an opposite behavior when compared with the forward one. It implies that the dilepton production at backward rapidities should carry information of the nuclear effects at large Bjorken  $x$ , as well as that it is useful to investigate the  $p_T$  dependence of the observables in this kinematical regime.

PACS numbers: 27.75.-q, 13.85.Qk

---

\*Electronic address: marcos.betemps@ufrgs.br

†Electronic address: beatriz.gay@ufrgs.br

‡Electronic address: emmanuel.deoliveira@ufrgs.br

## I. INTRODUCTION

The hadron transverse momentum spectrum measured by the RHIC experiments [1] is one of the most accessible distributions carrying information about the high density nuclear environment. At forward rapidities, the transverse momentum distribution for hadrons presents results compatible with the Color Glass Condensate (CGC) description of the saturated regime at high energies [2]. These results are investigated through a nuclear modification ratio, which relates  $dAu$  and  $pp$  collisions. It is well known that the transverse momentum dependence of this ratio shows a pronounced Cronin peak at central rapidity, which is suppressed at forward ones. For central rapidities the Cronin peak is due to the multiple scatterings of the projectile constituents with the dense target. At large rapidities the Cronin peak suppression is understood as a signal of the saturation phenomena intrinsic of the Color Glass Condensate (CGC). However, at backward rapidities, the recently measured hadron nuclear modification ratio shows a pronounced peak [3], which should be due to final states interactions.

In this work the dilepton production at high energies in the backward rapidity region is investigated in the proton-nucleus and proton-proton collisions. The analysis at forward rapidities was already done [4] and the results show that the dilepton is also a suitable observable to investigate the Color Glass Condensate. Here, the interest to explore the backward region in the dilepton sector relies on the study of the nuclear effects at large and small  $x$  and on the comparison with the Cronin effect in this region. In this kinematical region, the nucleus interacts by means of large Bjorken  $x$  partons, and no saturation effects are expected consequently. In this regime, the proton interacts through the small  $x$  partons.

It has been shown [4] that the dilepton production at forward rapidities, analyzed in the context of the Color Glass Condensate in  $pAu$  collisions, presents the same features of the Cronin effect at forward rapidities, implying that this should be considered as an initial state effect. However, at backward rapidities, the Cronin peak present in the hadrons RHIC data [3] is still not understood, and could be related to final state effects. The dileptons analyzed in this kinematical region, since they do not interact strongly with the final environment, may not present the same behavior of the hadron spectra. Although it could imply the dilepton production to be symmetric when forward-backward regions are compared, in contrast to the different behavior of the hadron spectra in both regions, we verify that the dilepton

production at backward rapidities is strongly modified due to large  $x$  nuclear effects.

This work is organized as follows. In the next section the dipole approach is presented for the dilepton production at backward rapidities. In the Sec. 3 the nuclear partonic parametrizations employed in this work as well as a comparison between them are presented. In the Sec. 4 the results are discussed. Our conclusions are left to the last section of this work.

## II. DILEPTON PRODUCTION AT BACKWARD RAPIDITIES

To evaluate the dilepton production at backward rapidities, an adequate treatment of the approach employed for the forward ones needs to be considered. The investigation at forward rapidities in  $pA$  collisions requires to describe the nucleus as a high density saturated system (CGC), and the dileptons are produced by the decay of a virtual photon emitted by the quark from the proton, which interacts with the nuclear dense medium (basically a dipole approach in the momentum space with a specific configuration of the nucleus). In this case the dilepton cross section can be factorized considering the wave function of the fluctuation  $q\gamma^*$  and the interaction cross section of a quark with the nucleus, which takes into account the high density effects. However, at backward rapidities the nucleus interacts by means of large Bjorken  $x$  partons, being no more described by a high density QCD system. The proton interacts through very small  $x$  partons implying that the dipole picture could be applied in this kinematical regime.

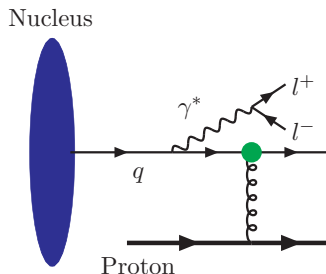


FIG. 1: In the dipole approach, dilepton production looks like a bremsstrahlung. A quark or an anti-quark from the projectile hadron (nucleus) scatters off the target color field and radiates a photon ( $\gamma^*$ ) with mass  $M$  (before or after the quark scatters), which subsequently decays into the lepton pair.

In the dipole approach at backward rapidities, the quark of the incident hadron (nucleus) fluctuates into a state containing a quark and a massive photon. The interaction with the target (proton) provides that the virtual photon is freed, decaying into a lepton pair [5] (one of the diagrams is shown in the Fig. 1).

We are interested in the study of the dilepton production in a region where the interaction time of the projectile quark with the proton target is much shorter than the  $q\gamma^*$  fluctuation time, meaning large coherence length. In order to apply the dipole picture at backward rapidities, we need to exchange the nucleus with the proton when comparing with the dipole picture at forward rapidities. In doing such procedure, the  $q\gamma^*$  fluctuation time will be larger than the interaction time, since the coherence length  $l_c$  has the dependence  $l_c \propto 1/x_1$  in the case studied here. Indeed, the coherence length is important in the study of nuclear targets, where it is a fundamental quantity controlling nuclear effects [6]. For the nuclear targets large coherence length needs to be reached if shadowing effect are under investigation, which implies that the approach should be applied only to smaller Bjorken  $x$  [7]. Another interesting point that arises here is that the  $p_T$  broadening due to the nuclear multiple scattering verified at forward rapidities [6] should not be present at backward rapidities, since the nuclear projectile will interact with a proton target and will not probe a large and very dense system.

The advantage of this formalism is that the dilepton cross section can be written in terms of the same color dipole cross section as small- $x$  Deep Inelastic Scattering (DIS). Although diagrammatically no dipole is present in bremsstrahlung, the dipole cross section arises from the interference of the two bremsstrahlung diagrams, as shown in Ref. [8] in a detailed derivation.

The cross section for the radiation of a virtual photon from a quark (with momentum fraction  $x_2$ ) of the nucleus scattering off a proton at high density at backward region can be written in a factorized form as [9, 10],

$$\frac{d\sigma^{DY_{back}}}{dM^2 dy d^2p_T} = \frac{\alpha_{em}^2}{6\pi^3 M^2} \int_0^\infty d\rho W(x_2, \rho, p_T) \sigma_{dip}(x_1, \rho), \quad (1)$$

where  $p_T$  is the dilepton transverse momentum,  $M$  is the dilepton mass,  $y$  the rapidity,  $\rho$  is the dipole transverse separation. The variables  $x_1$  and  $x_2$  are defined in the usual way  $x_{(1)} = \sqrt{\frac{M^2 + p_T^2}{s}} e^{\pm y}$ , with  $s$  being the squared center of mass energy. As can be seen from the definition of  $x_1$  and  $x_2$ , backward rapidities will provide large  $x_2$  and small  $x_1$ . We

are investigating dilepton production in  $pp$  and  $pA$  collisions. In a symmetric collision, the lab frame is equivalent to the center of mass frame considering colliders. In the case of asymmetric collisions, e.g.  $pA$ , the center of mass moves longitudinally in the lab frame. It provides that a largest interval in Bjorken  $x$  could be explored in the asymmetric collisions [11] if the lab frame is under consideration. In this work the ratio between  $pA$  and  $pp$  collisions will be investigated considering the rapidity in the lab frame.

Based on the dipole approach, the function  $W(x_2, \rho, p_T)$  is given by [9],

$$W(x_2, \rho, p_T) = \int_{x_2}^1 \frac{d\alpha}{\alpha^2} F_2^A\left(\frac{x_2}{\alpha}, M^2\right) \left\{ [m_q^2 \alpha^2 + 2M^2(1 - \alpha)^2] \left[ \frac{1}{p_T^2 + \eta^2} T_1(\rho) - \frac{1}{4\eta} T_2(\rho) \right] \right. \\ \left. + [1 + (1 - \alpha)^2] \left[ \frac{\eta p_T}{p_T^2 + \eta^2} T_3(\rho) - \frac{1}{2} T_1(\rho) + \frac{\eta}{4} T_2(\rho) \right] \right\}. \quad (2)$$

In the above equation  $\alpha$  is the momentum fraction of the quark carried by the virtual photon,  $\eta^2 = (1 - \alpha)M^2 + \alpha^2 m_q^2$ ,  $m_q$  is the quark mass ( $m_q = 0.2$  GeV) and the functions  $T_i$  are given by,

$$T_1(\rho) = \frac{\rho}{\alpha} J_0\left(\frac{p_T \rho}{\alpha}\right) K_0\left(\frac{\eta \rho}{\alpha}\right) \\ T_2(\rho) = \frac{\rho^2}{\alpha^2} J_0\left(\frac{p_T \rho}{\alpha}\right) K_1\left(\frac{\eta \rho}{\alpha}\right) \\ T_3(\rho) = \frac{\rho}{\alpha} J_1\left(\frac{p_T \rho}{\alpha}\right) K_1\left(\frac{\eta \rho}{\alpha}\right).$$

Here, a nuclear structure function  $F_2^A(\frac{x_2}{\alpha}, M^2)$  with a  $x_2$  dependence is considered in order to take into account the nuclear interaction. For  $pp$  collisions the nuclear structure function  $F_2^A(\frac{x_2}{\alpha}, M^2)$  needs to be replaced by the proton structure function  $F_2^p(\frac{x_2}{\alpha}, M^2)$ . The dipole cross section is evaluated with the argument  $x_1$  and the same dipole cross section extracted from the deep inelastic scattering HERA data should be applied.

The dipole cross section in the phenomenological model proposed by Golec-Biernat and Wüsthoff [12] (GBW), which has produced a good description of HERA data in both inclusive and diffractive processes, was employed here. It is constructed interpolating the color transparency behavior  $\sigma_{dip} \sim \rho^2$  for small dipole sizes and a flat (saturated) behavior for large dipole sizes  $\sigma_{dip} \sim \sigma_0$  (confinement). The expression has the eikonal-like form,

$$\sigma_{dip}(x_1, \rho) = \sigma_0 \left[ 1 - \exp\left(-\frac{\rho^2 Q_0^2}{4(x_1/x_0)^\lambda}\right) \right], \quad (3)$$

where  $Q_0^2 = 1$  GeV<sup>2</sup> and the three fitted parameters are  $\sigma_0 = 23.03$  mb,  $x_0 = 3.04 \times 10^{-4}$  and  $\lambda = 0.288$ .

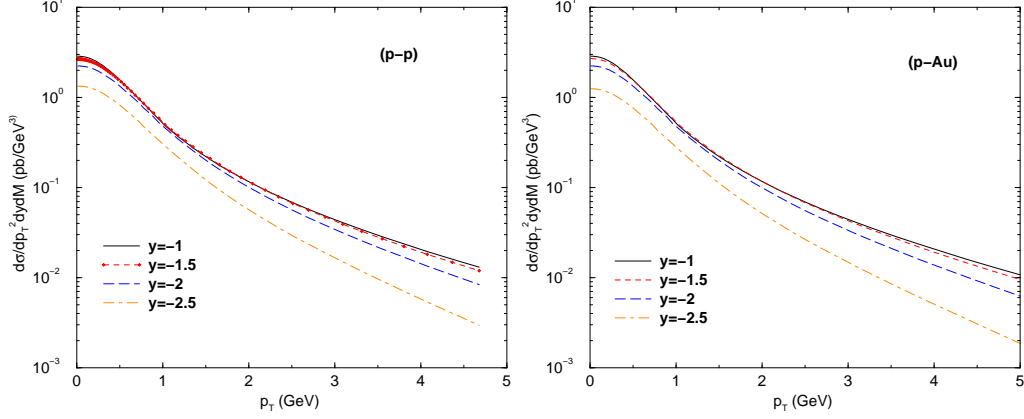


FIG. 2: Dilepton transverse momentum distribution for  $pp$  and  $pA$  (Au – considering EKS parametrization) collision at RHIC energies for dilepton mass  $M = 6$  GeV.

The  $pp$  and  $pAu$  transverse momentum distributions at RHIC energies for backward rapidities can now be evaluated, considering a specific parametrization to the nuclear structure function  $F_2^A(x, M^2)$  in the  $pA$  case. Two distinct parametrizations for the nuclear structure function will be used, which will be properly discussed in the next section. In this section EKS nuclear parametrization [13] was employed together with the GRV98 parton distribution function [14] in order to obtain the  $p_T$  distribution for the  $pA$  collision and the  $F_2^p(x, M^2)$  is obtained from the GRV98 parametrization for the  $pp$  collision. In the Fig. 2 the  $pp$  and  $pA$  transverse momentum distributions for RHIC energies are shown and significant visible differences between both distributions are not found. For this reason, the ratio between  $pA$  and  $pp$  cross section should be useful to investigate modifications in the nuclear cross section in comparison with the  $pp$  distribution. The ratio is defined in the following way

$$R_{pA} = \frac{d\sigma(pA)}{dp_T^2 dy dM} \bigg/ A \frac{d\sigma(pp)}{dp_T^2 dy dM}. \quad (4)$$

The ratio  $R_{pA}$  is normalized by  $1/A$ , since the nuclear parton distributions are normalized by this factor. The difference between  $pA$  and  $pp$  calculations are due to the nuclear structure function  $F_2^A$ , then any effect in the  $p_T$  or rapidity spectra should be related to the nuclear effects contained in this function.

The next-to-leading order calculation (NLO) in the collinear factorization could be evaluated and compared with the results in the dipole approach. However, the evaluation of the transverse momentum distribution in the collinear factorization is not a straightforward calculation and does not describe the normalization of the  $p_T$  Drell-Yan dileptons [15, 16].

A resummation of large logarithms in  $p_T/M$  [15, 16] or the introduction of an intrinsic transverse momentum [17] should be necessary to avoid the divergence of the differential cross section at  $p_T \ll M$ . New approaches have been suggested in order to describe the  $p_T$  spectra of the dilepton (for a good discussion see Ref. [18]), however, there is a strong dependence on phenomenological parameters. Considering, for instance, the intrinsic transverse momentum, the  $p_T$  distribution is dependent on a phenomenological parameter (see Ref. [8] for a comparison between the NLO calculations and the dipole approach, and Ref. [18] for a new approach). Of course, the ratio  $R_{pA}$  should be finite since the  $p_T$  divergence will be canceled, however, a more reliable result needs to consider finite spectra. This indicates that the dipole approach should be more adequate to investigate the low  $p_T$  dileptons at high energies, since there are no free parameters and the cross section is finite at low  $p_T$ .

For sake of completeness, it should be stressed that some limitations of the dipole approach at backward rapidities are in order. Here, the nucleus is considered by means of an integrated gluon distribution, however, at LHC energies and more central rapidities, the Bjorken  $x_2$  (nucleus) reaches values around 0.002, where the consideration of an integrated parton distribution could be questionable. At this high energy limit, the effects of finite transverse momentum of the incoming partons become important. A more robust treatment would need to include the transverse momentum of the partons from the nucleus in the initial state of the interaction. This should be done considering the  $k_T$  factorization approach [19], where the off-shell partonic cross sections are convoluted with  $k_T$  unintegrated parton densities  $f_a(x, k_T^2, \mu^2)$ . Considering dilepton production, the  $k_T$  factorization is investigated in the Ref. [20] and compared with a phenomenological intrinsic  $k_T$  approach ( $k_T$  factorization with on-shell partons), in order to describe the transverse momentum distribution of the Drell-Yan dilepton production. In spite of a reasonable data description, the  $k_T$  factorization overestimates the data and the intrinsic  $k_T$  approach depends on phenomenological parameters (two parameters).

For the reasons presented above, we have focused our analysis at backward rapidities, and not at more central ones. The use of the dipole approach together with the collinear factorization is justified as the goal of this work is to investigate the nuclear effects in the nuclear modification ratio  $R_{pA}$  for dileptons, using nuclear parametrizations to describe the  $F_2^A$ . In the next section the parametrizations for the nuclear structure function will be discussed and compared.

### III. NUCLEAR PARTON DISTRIBUTION FUNCTION

In this work the parametrizations for the nuclear parton distribution function (nPDF) proposed by Eskola, Kolhinen and Salgado (EKS parametrization) [13] and by D. de Florian and R. Sassot (nDS parametrization) [21] are considered in order to describe the nuclear effects in the  $F_2^A$ . In this section the main features of each parametrization will be discussed.

Both nuclear parton distribution functions provide a global fitting to fixed target experimental results, and consider the DGLAP equations for the  $Q^2$  evolution. The initial conditions are adjusted to describe the DIS in lepton-nucleus collisions and the dilepton production in proton-nucleus collisions. Both nPDFs are used to obtain an appropriated parametrization for the ratio  $R_{F_2}^A(x, Q_0^2) = F_2^A / AF_2^p$ , with

$$F_2^{A,p} = \sum_q e_q^2 [x f_q^{A,p}(x, Q_0^2) + x f_{\bar{q}}^{A,p}(x, Q_0^2)], \quad (5)$$

in which  $f_q^p(x, Q_0^2)$  are the free proton parton distributions and  $f_q^A(x, Q_0^2)$  are the nuclear distributions of parton flavor  $q$ . The parametrization for the parton distributions are constrained by charge, baryon number, and momentum conservation.

However, the method used by EKS and nDS differs with respect to their approaches to parametrize the nPDFs. In the EKS approach, the nuclear parton distributions are the free proton ones times a correction factor:  $f_q^A(x, Q_0^2) = R_q^A(x, Q_0^2) f_q^p(x, Q_0^2)$ , and all nuclear effects are enclosed in  $R_q^A(x, Q_0^2)$ . One consequence of this definition is that the nPDFs are null for  $x > 1$ , although they should be non-zero for  $x < A$ . On the other hand, nDS uses a convolution to relate nPDFs to the free proton PDFs:

$$f_q^A(x, Q_0^2) = \int_x^A \frac{dy}{y} W_q(y, A) f_q^p\left(\frac{x}{y}, Q_0^2\right), \quad (6)$$

in which  $W_i(y, A)$  contains the information about the nuclear effects. For instance, if nuclear effects are disconsidered,  $W_q(y, A) = A\delta(1 - y)$ .

The nuclear effects are verified by comparison of the nuclear structure function with the proton (or deuterium) structure function. In the Fig. 3 the prediction for the ratio  $F_2^A / AF_2^p$  is presented for both parametrizations. The figure can be divided in four regions of Bjorken- $x$  [22]. In the Fermi motion region  $x \gtrsim 0.8$ ,  $R_{F_2}^A$  is greater than 1 and increases with  $x$ . The EMC region  $0.3 \lesssim x \lesssim 0.8$  is characterized by  $R_{F_2}^A < 1$ . The antishadowing region  $0.1 \lesssim x \lesssim 0.3$ , and the shadowing region  $x \lesssim 0.1$  are defined by  $R_{F_2}^A > 1$ , and



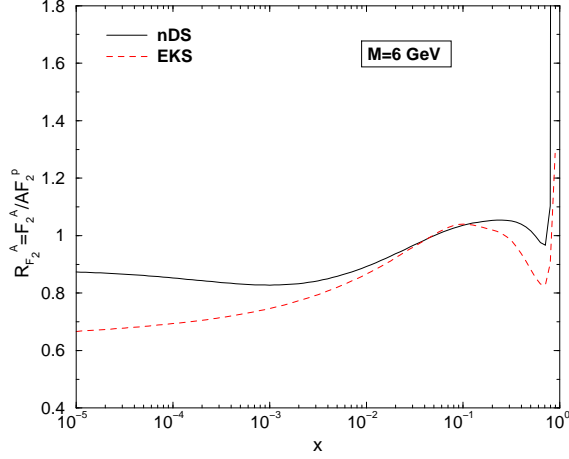


FIG. 3: Comparison between EKS and nDS parametrizations for the ratio  $F_2^A/F_2^p$  ( $A=\text{Au}$ ) for a dilepton mass (scale)  $M = 6$  GeV as a function of the Bjorken  $x$  of the nucleus.

$R_{F_2}^A < 1$ , respectively. The Fig. 3 shows that the parametrizations differ most in both ECM and shadowing regions, with EKS parametrization getting a lower ratio than nDS. The parametrizations are considered at the leading-order, since the approach employed here considers LO diagrams, without higher orders calculations. Indeed, the dipole cross section should carry some information about higher orders, but these properties are included in the phenomenological parametrization of the dipole cross section, in our case, the GBW parametrization [12].

In the next section, the results for dilepton production will be explored, considering both parametrizations for the nuclear parton distribution presented in this section.

#### IV. RESULTS AND DISCUSSIONS

The results for transverse momentum and rapidity distributions for the dilepton production (with mass  $M = 6$  GeV) at RHIC ( $\sqrt{s} = 200$  GeV) and LHC ( $\sqrt{s} = 8.8$  TeV) energies at backward rapidities will be discussed.

The ratio  $R_{pA}$  was evaluated at RHIC and LHC energies, and in the Figs. 4 and 5 the results are shown in 3D plots for rapidity and  $p_T$  spectra, considering the EKS and nDS parametrizations. The behavior of the ratio  $R_{pA}$  reflects the  $x_2$  dependence of the ratio  $F_2^A/F_2^p$ , presented in the Fig. 3.

At RHIC energies a weak dependence of the ratio on the transverse momentum is verified,

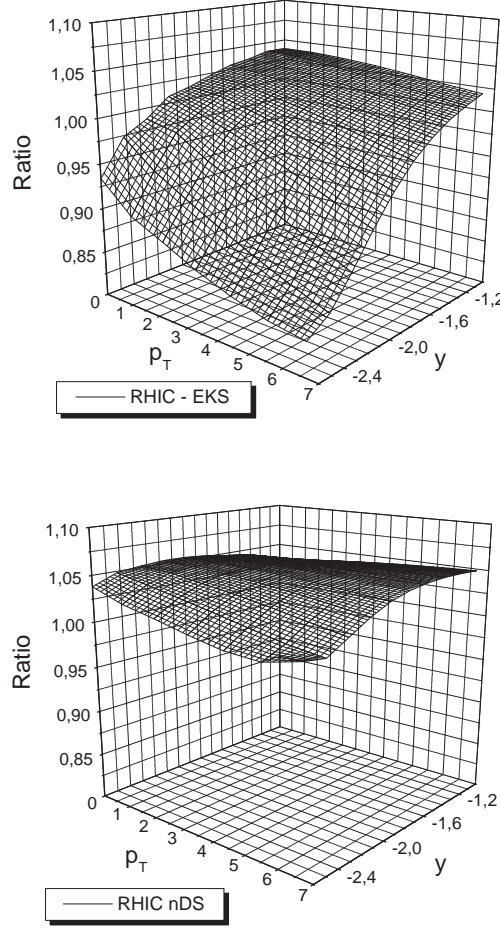


FIG. 4: Ratio  $R_{pA}$  for RHIC energies considering the EKS and nDS parametrizations.

and in general the ratio reaches smaller values at large  $p_T$ , being this more evident with the EKS parametrization. Concerning the rapidity spectra, the EKS parametrization predicts a strong suppression of the ratio at very backward rapidities and large  $p_T$ , in comparison with the nDS parametrization, which predicts an almost flat behavior.

To explain such results it is necessary to know the range of  $x_2$  values in the rapidity and  $p_T$  spectra at RHIC. For RHIC energies considering rapidities from -1 to -2.6, and  $p_T$  from 1 to 7, the  $x_2$  range is between 0.08 and 0.5, respectively, meaning that for more backward rapidities, partons with larger  $x_2$  are being probed. The nuclear effects that appear in the  $F_2^A$  at this  $x_2$  range are mainly due to EMC effect (reduction of the ratio  $R_{F_2}^A$  as  $x_2$  increases, see Fig. 3), which provides the reduction of the ratio  $R_{pA}$  at lower rapidities in the Fig. 4.

Concerning the  $p_T$  spectra,  $x_2$  increases with  $p_T$ , and as the region probed here is related to the EMC effect, the result is a reduction of the ratio  $R_{pA}$  as  $p_T$  increases. The large suppression of the ratio  $R_{pA}$  of the EKS prediction in comparison with the nDS in the Fig. 4 is a consequence of the large difference in the  $R_{F_2}^A$  predictions of the parametrizations in the EMC effect region.

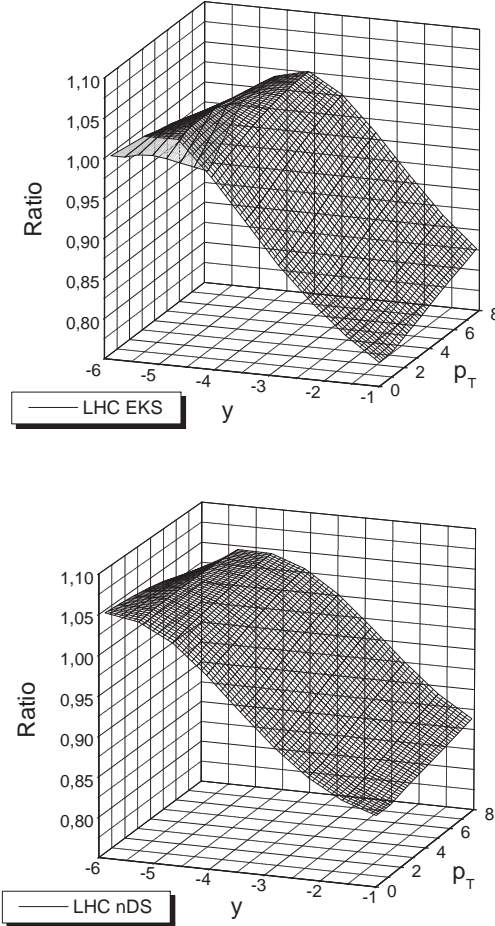


FIG. 5: Ratio  $R_{pA}$  for LHC energies considering the EKS and nDS parametrizations.

At LHC energies (Fig. 5) the rapidity spectra present a peak at intermediated rapidities, which is more pronounced in the EKS parametrization in comparison with the nDS parametrization. The  $R_{pA}$  transverse momentum dependence presents two distinct behaviors: for very backward rapidities the ratio decreases as  $p_T$  increases and for more central rapidities the ratio  $R_{pA}$  increases with  $p_T$ .

For LHC energies, rapidities from -1 to -6, and  $p_T$  from 1 to 7, the  $x_2$  range is between 0.002 and 0.3, respectively. Here we verify that not only large  $x$  of the nucleus is been probed, but small  $x$  too. The  $x_2$  range probed at LHC provides that shadowing and antishadowing effects are present. The peak at intermediate rapidities is related to the antishadowing effect and the suppression at more central rapidities is related to the shadowing effect. The  $p_T$  spectra is more involved since the ratio  $R_{pA}$  presents different behaviors. For more backward rapidities the ratio is reduced for large  $p_T$  ( $x_2$  in the antishadowing region, near to EMC region). For more central rapidities, the ratio increases for large  $p_T$ , since the  $x_2$  is in the shadowing region.

Comparing the predictions from the EKS and nDS parametrizations, in the Fig. 3 the EKS parametrization predicts more pronounced antishadowing, which explains the results found here for the ratio  $R_{pA}$  at LHC energies (Fig. 5). Our results presented for LHC energies show that dilepton carries information about the large and small  $x$  regime of the nuclear environment. The distinct nuclear effects are verified in rapidity and  $p_T$  spectra for the dilepton production at backward rapidities, for RHIC and LHC energies, following the  $x$  region involved.

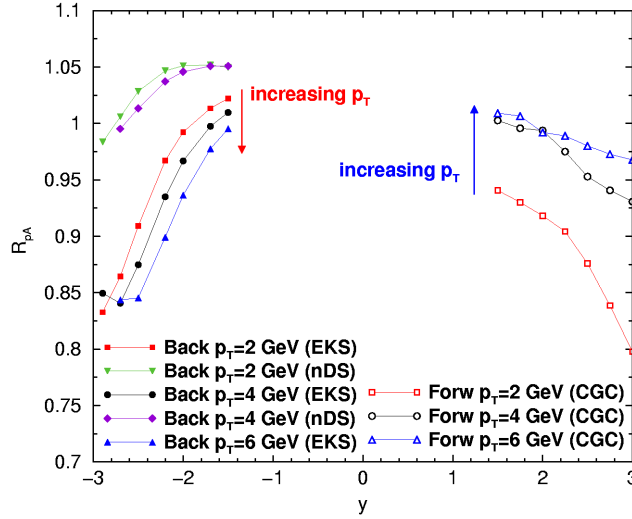


FIG. 6: Comparing the ratio  $R_{pA}$  for dileptons at backward and forward rapidities for RHIC energies, considering the EKS and nDS nuclear parametrizations at backward, and the CGC predictions at forward [4].

In order to compare the results presented in this work, with the previous results from the forward region [4], in the Fig. 6 the ratio  $R_{pA}$  for RHIC energies is shown for positive

and negative rapidities. The ratio presents different behaviors concerning the transverse momentum dependence. While at forward rapidities the saturation phenomena implies that the ratio  $R_{pA}$  increases at large  $p_T$ , at backward rapidities the ratio  $R_{pA}$  decreases as large  $p_T$  is reached. This distinct behavior is associated with the large  $x$  nuclear effects present at backward rapidities.

## V. CONCLUSIONS

The nuclear modification ratio  $R_{pA}$  for the dilepton production was investigated for  $p_T$  and backward rapidity spectra in the dipole picture for RHIC and LHC energies. We have verified a strong dependence of the nuclear modification ratio with the nuclear effects. The results presented in this work are explained by the dependence of the nuclear structure function ratio  $R_{F_2}^A$  on the Bjorken  $x$ . The hadron production was investigated at backward rapidities by PHENIX collaboration at RHIC [3] presenting the data on the nuclear modification ratio. The results present an enhancement in the nuclear modification ratio for  $1.5 < p_T < 4.0$ , which still demands some caution, once there are some data uncertainties and a discrepancy between analysis methods of the data. The results presented in this work for dileptons indicate that the enhancement in the hadron spectra at backward rapidities could be mainly due to final states, since, the initial state effects investigated here do not provide such behavior. Moreover, the dilepton at backward rapidities is a suitable observable to understand and quantify the nuclear effects at large and small Bjorken  $x$ . Additionally, the transverse momentum dependence of the ratio  $R_{pA}$  is strongly modified at RHIC energies, if forward and backward rapidities are compared, due to distinct  $x$  regions being probed.

## Acknowledgements

We thank Boris Kopeliovich for fruitful discussions during his visit to GFPAE at the occasion of the I LAWHEP and for a careful reading of this manuscript. This work was

partially supported by CNPq, Brazil.

---

- [1] BRAHMS collaboration, R. Debbe, J. Phys. G 30, S759 (2004). I. Arsene *et al.* The BRAHMS Collaboration, Phys. Rev. Lett. 93, 242303 (2004).
- [2] J. Jamal-Jalilian, Y. Kovchegov, Prog. Part. Nucl. Phys. 56, 104 (2006).
- [3] S.S. Adler, et al. PHENIX Collaboration. Phys. Rev. Lett. 94, 082302 (2005).
- [4] M. A. Betemps, M. B. Gay Ducati, Phys. Rev. D 70, 116005 (2004); Eur. Phys. J. C 43, 365 (2005); Phys. Lett. B 636, 46 (2006).  
F. Gelis and J. Jalilian-Marian, Phys. Rev. D 66, 094014 (2002).  
R. Baier, A. H. Mueller and D. Schiff, Nucl. Phys. A 741, 358 (2004).
- [5] B. Z. Kopeliovich, J. Raufeisen, A. V. Tarasov and M. B. Johnson, Phys. Rev. C 67, 014903 (2003).
- [6] M. B. Johnson, et al. Los Alamos ePrint arXiv hep-ph/0606126.
- [7] N. Armesto, Eur. Phys. J. C 26, 35 (2002).
- [8] J. Raufeisen, J.C. Peng, G.C. Nayak, Phys. Rev. D 66, 034024 (2002).
- [9] M. A. Betemps, M. B. Gay Ducati, M. V. T. Machado, J. Raufeisen, Phys. Rev. D 67, 114008 (2003).
- [10] B.Z. Kopeliovich, In proceedings *Workshop Hirschegg'95: Dynamical Properties of Hadrons in Nuclear Matter*. Ed. by H. Feldmeier and W. Nörenberg, GSI, Darmstadt, p. 102 (1995) [hep-ph/9609385];  
S.J. Brodsky, A. Hebecker, E. Quack, Phys. Rev. D 55, 2584 (1997).
- [11] N. Carrer, A. Daianese, ALICE-INT-2003-019, ePrint arXiv:hep-ph/0311225.
- [12] K. Golec-Biernat, M. Wüsthoff, Phys. Rev. D 59, 014017 (1999); Phys. Rev. D 60, 114023 (1999).
- [13] K.J. Eskola, V.J. Kolhinen and C.A. Salgado, Eur. Phys. J. C 9, 61 (1999); K.J. Eskola, V.J. Kolhinen and P.V. Ruuskanen, Nucl. Phys. B 535, 351 (1998).
- [14] M. Glück, E. Reya, A. Vogt, Eur. Phys. J. C 5, 461 (1998).
- [15] J. C. Collins, D. E. Soper and G. Sterman, Nucl. Phys. B 250, 199 (1985).  
J. w. Qiu and X. f. Zhang, Phys. Rev. Lett. 86, 2724 (2001).
- [16] G. I. Fai, J. w. Qiu and X. f. Zhang, Phys. Lett. B 567, 243 (2003).

- [17] G. Altarelli, G. Parisi and R. Petronzio, Phys. Lett. B 76, 351 (1978).
- [18] O. Linnyk, S. Leupold, U. Mosel, ePrint arXiv:hep-ph/0607305.
- [19] S. Catani, M. Ciafaloni, F. Hautmann, Phys. Lett. B 242, 97 (1990); Nucl. Phys. B 366, 135 (1991).  
J. Collins, R. Ellis, Nucl. Phys. B 360, 3 (1991).
- [20] O. Linnyk, S. Leupold, U. Mosel, Phys. Rev. D 71, 034009 (2005).
- [21] D. de Florian and R. Sassot, Phys. Rev. D 69, 074028 (2004).
- [22] N. Armesto, ePrint arXiv:hep-ph/0604108.